Heliyon 10 (2024) e23336

Contents lists available at ScienceDirect

Heliyon

journal homepage: www.cell.com/heliyon

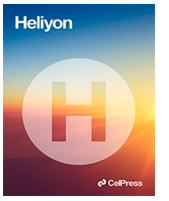

Kaempferol and nicotiflorin ameliorated alcohol-induced liver injury in mice by miR-138-5p/SIRT1/FXR and gut microbiota

Jian Ge [*,1], Guangmei Li [1], Zhaowen Chen [1], Weijia Xu, Xuanhao Lei, Shengnan Zhu

College of Life Sciences, China Jiliang University, 258 XueYuan Street, XiaSha Higher Education Zone. Hangzhou, 310018, Zhejiang Province, People's Republic of China

ARTICLE INFO

Keywords:
Nicotiflorin
Kaempferol
Alcohol-induced liver injury
miR-138-5p/SIRT1/FXR signaling pathway
Gut microbiota

ABSTRACT

Aims: Excessive alcohol consumption can lead to alcoholic liver diseases (ALDs). *Tetrastigma hemsleyanum Diels et Gilg* is a rare Chinese medicinal herb. *Tetrastigma hemsleyanum Diels et Gilg* has been validated to be highly effective for treating hepatitis. Kaempferol and nicotiflorin are two highly representative flavonoids, which have exhibit therapeutic effects on liver disease. Therefore, the protective mechanism of kaempferol and nicotiflorin on alcohol-induced liver injury were investigated.

Main methods: Forty mice were used in this study. After treatment of Kaempferol and nicotiflorin, serum and liver were collected and used for determination of biochemical indicators, H&E staining, and molecular detection. The interaction of miRNAs from serum extracellular vehicles (EVs) with mRNAs and 16S rRNA sequencing of gut microbiota were also investigated.

Key findings: The results showed that kaempferol and nicotiflorins significantly ameliorated alcohol-induced liver damage and observably regulated gut microbiota. Specifically, the levels of malondialdehyde (MDA) and CYP2E1 in the liver significantly reduced, and the activity of superoxide dismutase (SOD) and glutathione (GSH) in the liver evidently increased. They also significantly relieved liver oxidative stress and lipid accumulation by suppressing miR-138-5p expression, inversely enhancing deacetylase silencing information regulator 2 related enzyme-1 (SIRT1) levels and then decreasing farnesoid X receptor (FXR) acetylation, which then modulated Nrf2 and SREBP-1c signaling pathways to regulate oxidative stress and lipid metabolism induced by alcohol.

Significance: Kaempferol and nicotiflorin reduced alcohol-induced liver damage by enhancing alcohol metabolism and reducing oxidative stress and lipid metabolism. The intestinal microorganism disorder was also ameliorated after oral kaempferol and nicotiflorin.

1. Introduction

Alcohol abuse is the main risk factor for liver disease and liver-related death [1,2]. Excessive drinking can lead to alcoholic liver diseases (ALDs) [3]. Some studies have further shown that drinking can cause an imbalance in the gut microbiota, increasing intestinal permeability and bacterial translocation, thereby inducing ALDs. The current treatment methods for ALD depend on the staging of ALD and the acceptability, safety, and tolerability of treatment, such as abstinence from alcohol [4]. Thus, developing new liver-protective

* Corresponding author.
E-mail address: gejian@cjlu.edu.cn (J. Ge).
[1] These authors contributed equally to this work.

https://doi.org/10.1016/j.heliyon.2023.e23336
Received 31 August 2023; Received in revised form 30 November 2023; Accepted 30 November 2023
Available online 6 December 2023

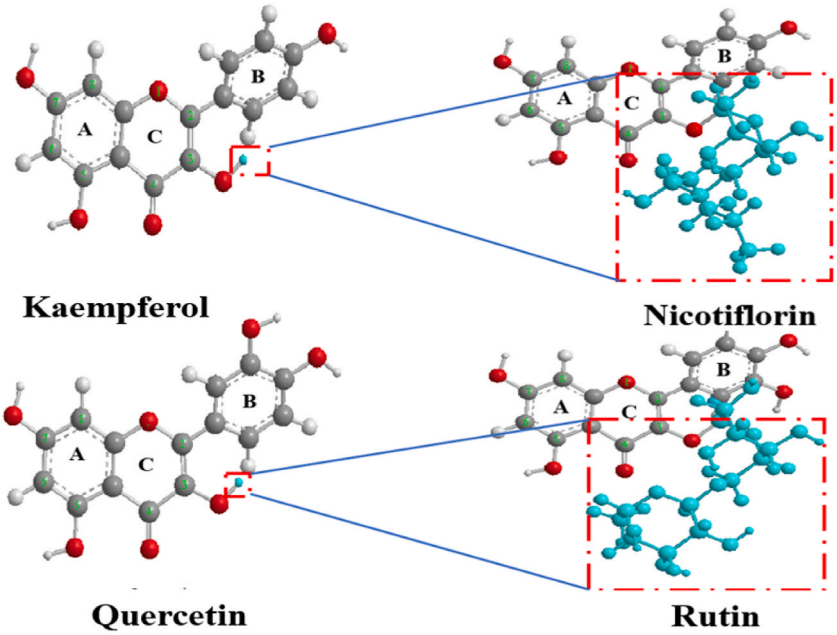

Fig. 1. Comparison of flavone structures.

components is important for ALD treatment.

A traditional Chinese herb called *Tetrastigma hemsleyanum Diels et Gilg* has medicinal effects. Plants have been proven to have many benefits, such as antioxidant ability and protection of the liver from chemical damage [5]. The root has many flavonoids, which have hypoglycemic, hypolipidemic, and antioxidative effects [6,7]. The liver harm from alcohol is primarily caused by oxidative damage. The antioxidant activity of *T. hemsleyanum* is reportedly closely related to flavonoids [8].

The purpose of this study was to explore whether *T. hemsleyanum* has a protective effect on alcoholic liver injury from the specific ingredients of total flavonoids in *T. hemsleyanum*. However, the components of total flavonoids are very complex, and explaining the mechanism is difficult. Combined with the content quantification of flavonoid monomers in *T. hemsleyanum* by HPLC, the contents of four monomers in *T. hemsleyanum* roots were found to decrease in the following order: nicotiflorin > rutin > kaempferol > quercetin. After observing the structures of the four flavonoids (Fig. 1), we found that the chemical structure of nicotiflorin was similar to that of kaempferol. Studies on rutin and quercetin for alcoholic liver injury are extensive [9–12]. However, no paper has reported on nicotiflorin and kaempferol with regard to their effect on alcohol-induced liver injury and the underlying mechanism.

2. Material and methods

2.1. Reagents and chemicals

Kaempferol was purchased from Nanjing Qingyuan Reagents Co. (Nanjing, China; batch number: 520-18-3-2022, 98.0 %). Nicotiflorin was purchased from Nanjing Qingyuan Reagents Co. (Nanjing, China; batch number: 403861-33-6-2022, 98.0 %). Glutathione (GSH) enzymatic activities, superoxide dismutase (SOD), aspartate transaminase (AST), alanine *trans*-aminase (ALT), triglyceride (TG), cytochrome P450 2E1 (CYP2E1), and total cholesterol (TC) ELISA kits were purchased from Thermo Fisher Co., Ltd.

2.2. Animal and treatment

Healthy mice (18–22 g) were purchased from Shanghai SLAC Laboratory Animal Co., Ltd. These mice were stored in a humidity- and air-controlled environment. The animals had free access to feed and water throughout the experiment. This research was approved by the Animal Experiment Ethics Committee of China Jiliang University (2023-003) and conformed to animal protection, welfare and ethical principles.

After a week of adaptive feeding, 40 mice were divided into four groups: control (CK), model (M), kaempferol, and nicotiflorin. Each group had ten mice (n = 10). The entire experimental period was divided into alcohol-adaptation (1–2 weeks) and alcohol-modeling (3–10 weeks) periods [13]. During the alcohol adaptation period, CK mice were given normal saline (blank solvent), whereas mice in the other groups (M, kaempferol, and nicotiflorin) were orally given 50° Beijing Red Star wine (50 % alcohol, v/v; 2, 4, 6, 8, and 10 g/kg BW) once a day. Specifically, mice in the M, kaempferol, and nicotiflorin groups were intragastrically administered for 3 days for every wine dose from 2 g/kg BW to 8 g/kg BW and 10 g/kg BW for 2 days during the alcohol adaptation period. The entire adaptation cycle was 2 weeks. Meanwhile, CK mice were dosed by gavage with normal saline. In the alcohol-modeling stage, CK mice

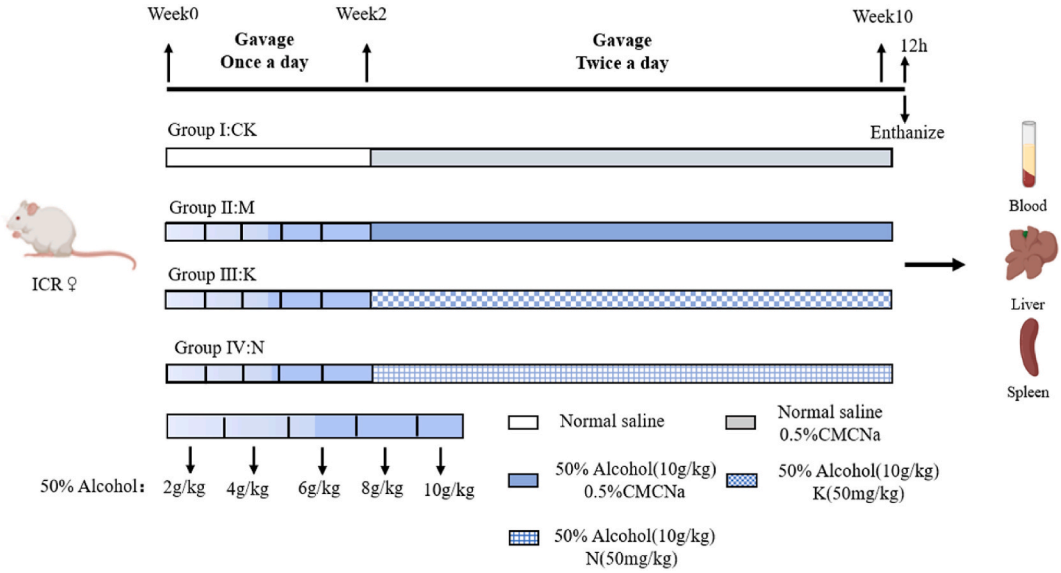

Fig. 2. Experimental grouping and gavage.

Table 1
Real-time PCR primers.

Gene	Genbank Accession	Primer Sequences(5′to3′)	Size(bp)
Mouse GAPDH	GU214026.1	GAAGGTCGGTGTGAACGGATTTG CATGTAGACCATGTAGTTGAGGTCA	127
Mouse SIRT-1	NM_019812.3	GGGAACCTTTGCCTCATCTACATT CACCACCTAGCCTATGACACA	90
Mouse SREBP-1c	NM_011480.3	CCCGGCTATTCCGTGAACAT GCAGATATCCAAGGGCATCTGA	111
mmu-miR-22-3p-RT	MIMAT0000531	GTCGTATCCAGTGCAGGGTCCGAG GTATTCGCACTGGATACGACACAGTT	60
mmu-miR-22-3p-F	MIMAT0000531	GCGAAGCTGCCAGTTGAAG	
mmu-miR-138-5p-RT	MIMAT0000150	GTCGTATCCAGTGCAGGGTCCGAGG TATTCGCACTGGATACGACCGGCCT	61
mmu-miR-138-5p-F	MIMAT0000150	GCGAGCTGGTGTTGTGAATC	
U6	M10329.1	GTCGTATCCAGTGCAGGGTCCGAGG TATTCGCACTGGATACGACGTCATCC	107
U6–F	M10329.1	CGCTTCGGCAGCACATATACTAA	
Universal reverse primer (micro-R)	/	AGTGCAGGGTCCGAGGTATT	/

were dosed by gavage with normal saline and 0.5 % carboxymethylcellulose sodium (CMC-Na) at a dose of 20 mL/kg BW. Mice in the Model group were given 50° wine at a dose of 10 g/kg BW and 0.5 % CMC-Na at a dose of 20 mL/kg BW for 8 weeks. Kaempferol group mice were treated with 50° wine at a dose of 10 g/kg BW and kaempferol at a dose of 50.0 mg/kg BW dissolved in 0.5 % CMC-Na for 8 weeks. The nicotiflorin group was treated with 50° wine at a dose of 10 g/kg BW and nicotiflorin at a dose of 50.0 mg/kg BW dissolved in 0.5 % CMC-Na for 8 weeks. After the last administration of alcohol and kaempferol or nicotiflorin, we fasted the experimental mice for half a day. Then, the mouse serum, liver, and spleen were collected. The specific grouping and gavage are shown in Fig. 2, and the intragastric volumes were adjusted according to mouse body weight

2.3. Determination of biochemical indicators in tissues and serum

Various ELISA kits were used to measure the levels of ALT, AST, TG, and Tc in serum, and the enzymatic activities of MDA, T-SOD, GSH-Px, and CYP2E1 in liver tissues were assayed according to the kit manufacturer's instructions. First, anticoagulant tubes were used to collect the blood supernatant. Then, the centrifuge tube was placed into a centrifuge for centrifugation (1500×*g* for 10 min, 4 °C). Serum was collected to determine the levels of ALT, AST, TC, and TG. At the same time, 1 g of liver tissue was added to a glass homogenizer containing 5 ml of precooled physiological saline for homogenization. The samples were homogenized in an ice bath, and the supernatant was collected for centrifugation (3000×*g* for 10 min, 4 °C). Then, the kit was used to determine the enzymatic activities of MDA, T-SOD, GSH-Px, and CYP2E1.

Table 2
Antibodies used for western blotting.

Antibody	Company	Dilutions
Ac-FXR	Abcam ab155124	1: 2000
p-Nrf2	Thermo Fisher PA5-67520	1:1000
GAPDH	Abcam ab181602	1: 10000

2.4. Histological analysis of the liver

Liver tissue (approximately 5 mm^3) in the same position was collected. PBS was used to flush the liver. Finally, the liver was placed in 10 % formalin neutral fixative solution for 48 h. Thereafter, paraffin was used to embed the tissues. Then, the tissues were sliced into 4 μm sections and used hematoxylin–eosin (H&E) staining. Finally, stained sections were observed under a microscope.

2.5. Quantitative real-time PCR assay

RT−qPCR was used to measure the mRNA expression of SIRT-1 and SREBP-1c in liver tissues. According to the manufacturer's protocol, total RNA was extracted by using a TRIzol® Plus RNA Purification Kit (Thermo Fisher, USA). Following the manufacturer's instructions, cDNA was synthesized using SuperScript™ III First-Strand Synthesis SuperMix for qRT−PCR (Thermo Fisher, USA). the primer sequences were listed in Table 1. The amplification method we adopted mainly involves several steps. First, we performed an initial denaturation (95 °C for 1 min). Second, we performed 40 cycles of denaturation (95 °C for 15 s). Then, annealing and extension were performed (95 °C for 15 s). According to the manufacturer's instructions, real-time PCR was performed with PowerUp™ SYBR™ Green Master Mix (Applied Biosystems, USA). Relative expression levels of target genes were normalized to GAPDH, evaluated by the $2^{-\Delta\Delta Ct}$ method (Lival and Schmittgen , 2001) and given as a ratio to control in the experiment.

2.6. Western blot assay

RIPA buffer (Thermo Fisher, USA) supplemented with Protease and Phosphatase Inhibitor Cocktail (Thermo Fisher, USA) were used to extract the protein from tissues. Then, protein was quantified by using a BCA protein assay kit (Beyotime Biotechnology, China). Each lane of the SDS−PAGE gel loaded approximately 50 μg of protein and transferred to a Hybond-P PVDF membrane (GE Healthcare, USA). 5 % nonfat milk in Tris-buffered saline containing 0.1 % Tween-20 was used to block the membranes. The membranes were then incubated at 4 °C overnight with the primary antibodies (Table 2). HRP-labeled goat anti-rabbit secondary antibody (1:5000, Thermo Fisher, USA) was used to make the Protein expression was visualized on X-ray films by SuperSignal West Dura Extended Duration Substrate (Thermo Fisher, USA). Image-Pro Plus 6.0 software was used to quantitate band intensities.

2.7. Isolation and characterization of serum extracellular vehicles (EVs)

The ultrafast centrifugation method was used to extract serum EVs. The collected blood was centrifuged (2000×*g* for 30 min) and discarded the supernatant. Then, 0.2 ml of serum was added to 0.04 ml of serum exosome separation solution and incubated the mixture at 4 °C for 0.5 h. Then, a Beckman L-100XP supercentrifuge (Brea, CA, USA) was used to centrifuge the supernatant (10000×*g* for 10 min, 4 °C). The supernatant was discarded, and the precipitates were centrifuged (100000×*g* for 5 min, 4 °C) again after being washed and suspended in PBS. Finally, we centrifuged the precipitates at 10000×*g* for 5 min at 4 °C and discarded the residual liquid. After that, PBS was used to resuspend the extracellular precipitate to obtain the serum extracellular precipitate. Then, the exosomes were characterized using a transmission electron microscopy system (HT7700, Hitachi Instruments Co., Ltd., Shanghai, China). Flow Nano-Analyzer N30E (Xiamen Fuliu Biological Technology Co., Ltd., Xiamen, China) was used to detect the average particle size of EVs. Meanwhile, Western blotting was used to identify EV-labeled protein tetraspanins (CD9 and CD63) and endosome or membrane-binding proteins (TSG101).

2.8. miRNA prediction

miRNAs in mammals exert posttranscriptional regulation by binding to the 3′-UTR of the transcript sequence. Thus, using TargetScan (https://www.targetscan.org/vert) and miRanda (www.microrna.org), we speculated that SIRT1 was a target gene of some miRNAs from EVs. All miRNAs related to the SIRT1 gene in mice were analyzed in miRDB. To ensure the reliability of the regulation, all SIRT1-related miRNAs were input into TargetScanMouse for further verification. Finally, miR-22-3p and miR-138-5p were screened for possible interactions with SIRT1.

2.9. miRNA levels in EVs were detected by RT-qPCR

According to the instructions of the PureLink ® miRNA Isolation Kit and SuperScript™ III Reverse Transcriptase kit, miRNAs were extracted from EVs, and the reverse transcription of miRNA stem ring primer sequences isum exosomes of mice in each group. The reverse-transcription primer sequence and the RT−qPCR primer sequences are shown in Table 1.

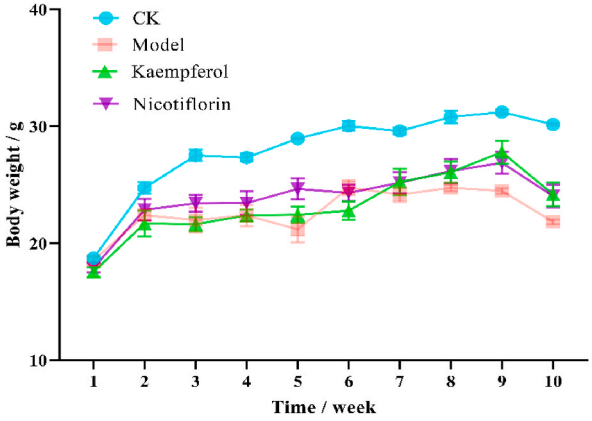

Fig. 3. Body weight gain of mice.

Table 3
Organ index in mice.

Name	Liver weight (g)	Liver index	Spleen weight (g)	Spleen index
CK	1.16 ± 0.09^{a}	4.63 ± 0.24^{a}	0.11 ± 0.01^{a}	0.25 ± 0.02^{a}
Model	1.51 ± 0.14^{b}	5.57 ± 0.25^{b}	0.16 ± 0.01^{b}	0.44 ± 0.01^{b}
Kaempferol	0.95 ± 0.08^{a}	3.71 ± 0.22^{c}	0.08 ± 0.02^{a}	0.26 ± 0.04^{a}
Nicotiflorin	1.10 ± 0.16^{a}	3.49 ± 0.37^{c}	0.09 ± 0.02^{a}	0.28 ± 0.03^{a}

Note: ($n = 8$) The same letters indicate no significant difference between groups ($p > 0.05$), and different letters indicate significant differences between groups ($p < 0.05$).

2.10. Dual-luciferase reporter gene assay

To confirm the targeting relationship between miR-138-5p and SIRT1, SIRT1 3′-UTR fragments were shown to interact with miR-138-5p putative binding sites. 293T cells were cultured in 96-well plates at a density of 5×10^4 cells/ml. Overnight, all these cells were cotransfected with pmirGLO-SIRT1 WT or MUT and miR-138-5p mimics or NC. The firefly and Renilla luciferase activities were determined with the Dual-Luciferase Reporter Assay System (Promega Co., Ltd., USA) according to the operating guidance after 48 h of culture. Then, firefly luciferase activity was normalized according to Renilla luciferase activity.

2.11. Bacterial DNA extraction and 16S rRNA sequencing

Cecal tissues were collected and put into a −80 °C refrigerator. After that, 200 mg of sample were used to extract the microbial DNA. PCR was used to amplify the 16S RNA gene V4–V5 regions. The PCR products were analyzed and separated by electrophoresis on a 2 % agarose gel. Then, Illumina NovaSeq 6000 platform was used to sequence and analyze the 16S rRNA gene clone library. And the sequencing data from our study in this paper were deposited in NGDC Sequence Read Archive (SRA) associated with BioProject ID PRJCA018703 (https://ngdc.cncb.ac.cn/search/?dbId=&q=PRJCA018703).

2.12. Statistical analysis

SPSS 20.0 (IBM, Armonk, NY, USA) was used to analyze all data by one-way ANOVA. Meanwhile, it can be expressed as the mean ± standard deviation. To examine the statistical significance among groups, we used Tukey's test for post hoc multiple comparisons. $p < 0.05$ was set as statistical significance.

3. Results

3.1. Kaempferol and nicotiflorin ameliorated organ index and body weight gain

Analysis of the mouse growth curve showed that during the 1–2 weeks alcohol adaptation period, the weight of mice in all groups increased normally, and they were healthy and gradually adapted to alcohol stimulation. Mouse modeling revealed that the weight gain of model mice was slow, whereas that of kaempferol and nicotiflorin mice was higher than that of the model group. All of them were lower than that of the CK group. In particular, the weight gap was very obvious at 8–10 weeks, and long-term drinking stimulation led to poor growth and weight loss, whereas kaempferol and nicotiflorin effectively relieved the mouse weight loss caused by alcohol (Fig. 3).

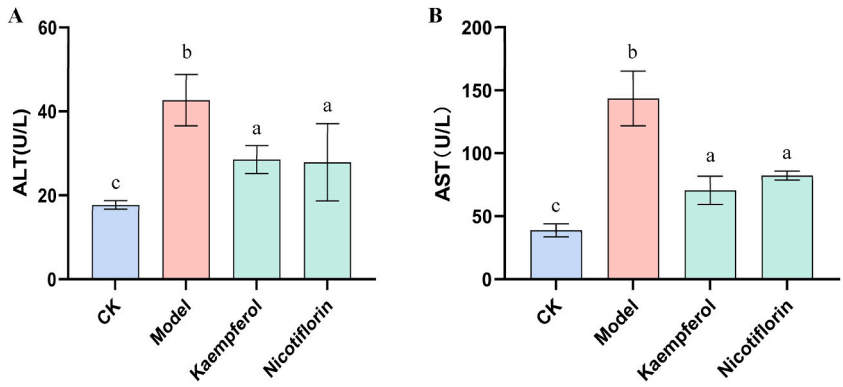

Fig. 4. Effects of kaempferol and nicotiflorin on serum concentrations of ALT (A), AST (B)
Note: ($n = 8$) The same letters indicate no significant difference between groups ($p > 0.05$), and different letters indicate significant differences between groups ($p < 0.05$).

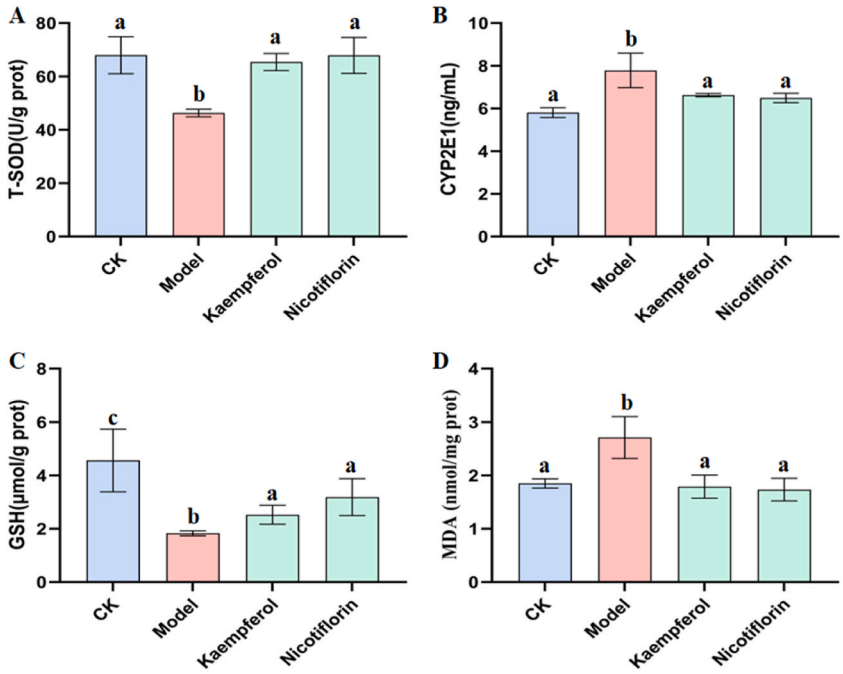

Fig. 5. Levels of T-SOD (A), CYP2E1 (B), GSH (C), and MDA (D) in liver
Note: ($n = 8$) The same letters indicate no significant difference between groups ($p > 0.05$), and different letters indicate significant differences between groups ($p < 0.05$).

Table 3 shows that the liver index in model mice was significantly higher than that in CK mice ($p < 0.05$), whereas the values in the kaempferol and nicotiflorin groups were obviously lower than those in the model and CK groups. The spleen index of 0.44 ± 0.01 in the Model group was significantly different from that in the CK group ($P < 0.05$). The spleen indices in the CK group and the kaempferol or nicotiflorin groups were all reduced, indicating that the intake of kaempferol or nicotiflorin alleviated spleen enlargement.

3.2. Kaempferol and nicotiflorin obviously recovered serum and liver indicators

As shown in Fig. 4A and B, the activities of serum ALT and AST in Model mice were significantly elevated compared with those in CK and were significantly decreased by kaempferol and nicotiflorin.

The antioxidant activities of kaempferol and nicotiflorin are shown in Fig. 5A–D. The levels of SOD and GSH-Px in livers were significantly reduced, and the MDA and CYP2E1 levels were significantly elevated in alcohol-treated mice compared with CK mice ($p < 0.05$) and were markedly restored by kaempferol and nicotiflorin.

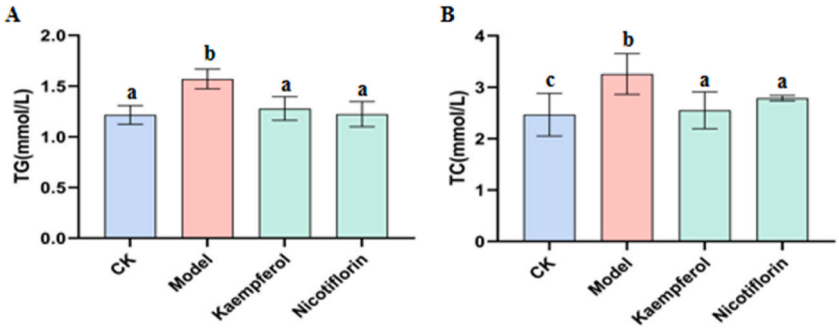

Fig. 6. Effects of kaempferol and nicotiflorin on serum concentrations of TC (A) and TG (B)
Note: ($n = 8$) The same letters indicate no significant difference between groups ($p > 0.05$), and different letters indicate significant differences between groups ($p < 0.05$).

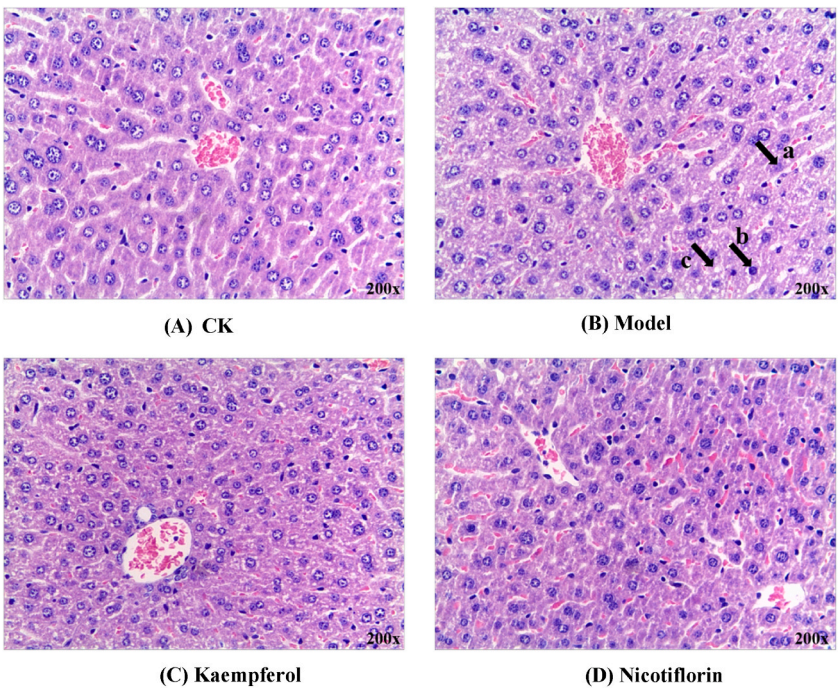

Fig. 7. Representative H&E stain of liver sections.
Note: a: nuclear solubilization; b: nuclear solidification; c: Fat drops.

3.3. Kaempferol and nicotiflorin observably regulated lipid metabolism

The levels of blood lipids are shown in Fig. 6A–B. In the model group, the TC and TG concentrations in blood significantly increased. Meanwhile, the TC and TG were decreased in the kaempferol and nicotiflorin group. These data indicated that kaempferol and nicotiflorin had an obvious lipid-lowering effect against liver dyslipidemia induced by alcohol intake.

3.4. H&E staining

The 200-fold magnification results of H&E staining are shown in Fig. 7. The nucleus of hepatocytes in CK was clearly visible in the center of the cell. The cell structure was complete, the arrangement was neat, and the liver tissue structure was not abnormal. Compared with CK, the liver cell arrangement was disordered in the liver pathological section of the Model group, and nucleus lysis (arrow a), nucleus contraction (arrow b), and fat droplets (arrow c) were observed, especially at the edge of the section. The liver tissue damage in the Model group mice was more serious, accompanied by mild fatty liver. It was obviously ameliorated by kaempferol and nicotiflorin. In these two groups, the edge of the liver cells was clear and regular, the morphology of the nucleus was regular, the boundary of the nucleus was clear, and the nucleus had no obvious contraction.

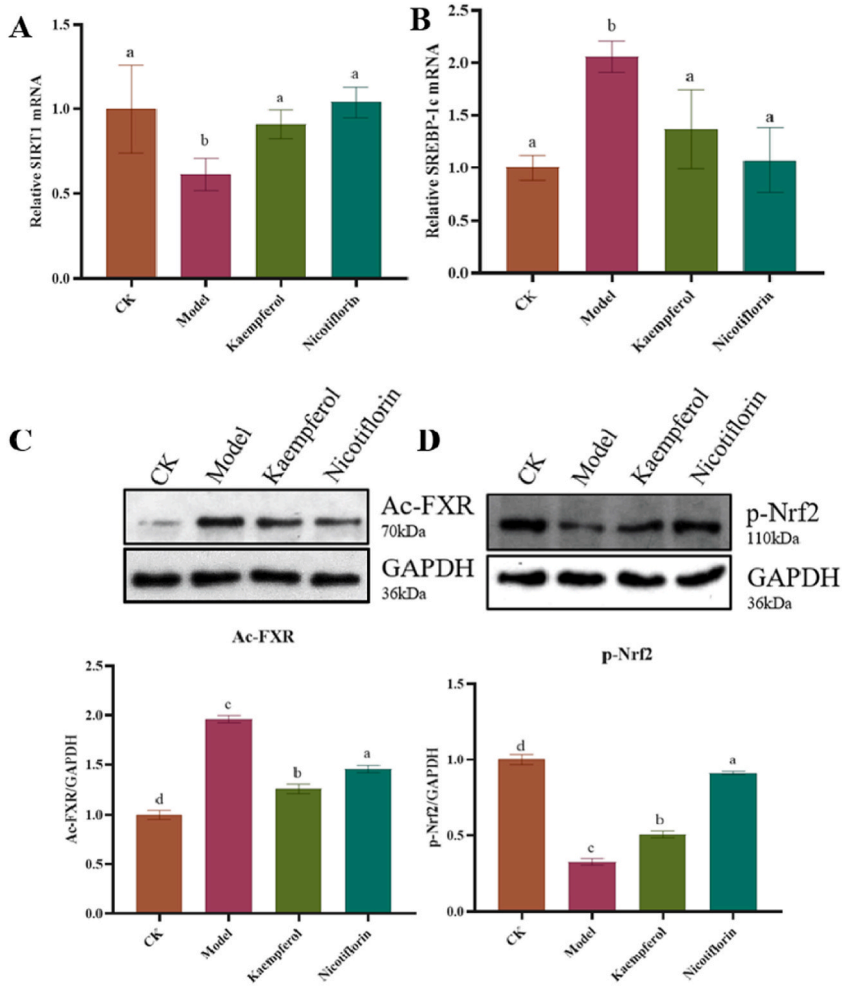

Fig. 8. (A) SIRT1 and (B) SREBP-1c mRNA levels in mouse livers were determined. (C) Acetylated endogenous FXR levels and Liver p-Nrf2 protein levels were analyzed by immunoprecipitation and Western blot assay.
Note: ($n = 5$) The same letters indicate no significant difference between groups ($p > 0.05$), and different letters indicate significant differences between groups ($p < 0.05$).

3.5. *Kaempferol and nicotiflorin significantly regulated FXR-Nrf2-mediated oxidative stress and FXR-SREBP-1c-mediated lipid metabolism*

Alcohol stimulation significantly downregulated the expression of SIRT1 mRNA in liver tissue, while SIRT1 mRNA levels were obviously upregulated in the kaempferol and nicotiflorin groups (Fig. 8A). Thus, FXR activity and phosphorylated Nrf2 (p-Nrf2) levels were all enhanced in the kaempferol and nicotiflorin groups (Fig. 8C–D). Accordingly, CYP2E1 and MDA levels were significantly downregulated (Fig. 5B–D), and the expression levels of downstream proteins, including SOD and GSH, were also significantly increased in the kaempferol and nicotiflorin groups (Fig. 5A–C). Therefore, these data suggested that kaempferol and nicotiflorin regulated the FXR-Nrf2 signaling pathway to suppress oxidative stress.

In Fig. 8B, oral kaempferol and nicotiflorin notably decreased the levels of SREBP-1c ($p < 0.05$). Consequently, the levels of TC and TG were obviously decreased in the kaempferol and nicotiflorin groups (Fig. 6A–B). These data indicated that kaempferol and nicotiflorin also modulated alcohol-induced lipid metabolism by FXR-SREBP-1c signaling.

3.6. *Identification of serum EVs*

As shown in the TEM observation in Fig. 9A, EVs had a saucer-like shape, and the particle sizes were distributed within the range of 50–150 nm (Fig. 9B). In addition, marker proteins (CD9, CD63, and TSG101) were also detected by Western blotting (Fig. 9C).

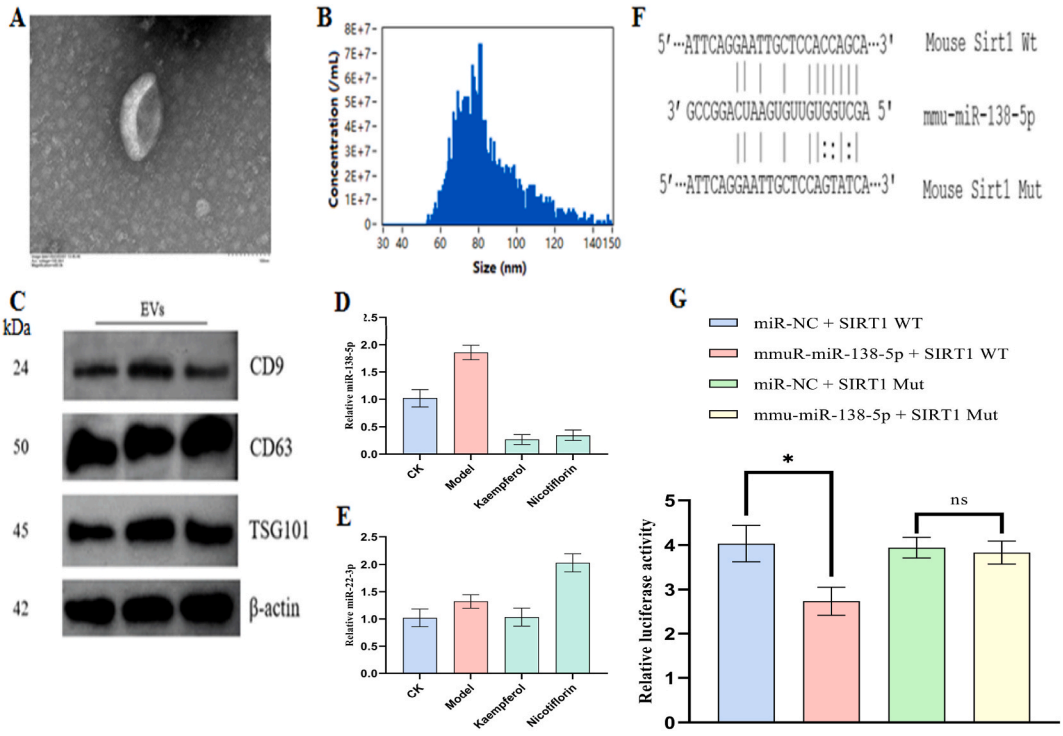

Fig. 9. Identification of serum extracellular vehicles
(A) Serum EVs observed by transmission electron microscopy (TEM). (B) Particle-size analysis. (C) Expression levels of CD9, CD63, and TSG101 determined by Western blot. miRNA expression level of EVs (D–E). SIRT1 is a molecular target of miR-138-5p. (F) Alignment of miR-138-5p and SIRT1 3′-UTR by computational prediction via the TargetScan and miRanda. (G) Dual-luciferase reporter assay was performed in RAW264.7 cells. *P < 0.05.
Note: ($n = 8$) The same letters indicate no significant difference between groups ($p > 0.05$), and different letters indicate significant differences between groups ($p < 0.05$).

3.7. *miRNA level in serum EVs were significantly regulated by kaempferol and nicotiflorin*

As shown in Fig. 9D, compared with the model group, the expression levels of miR-138-5p markedly decreased in the kaempferol group and the nicotiflorin group ($P < 0.01$). In Fig. 9E, the levels of miR-22-3p also significantly decreased in the kaempferol group ($P < 0.05$), whereas the levels obviously increased in the nicotiflorin group ($P < 0.05$). According to the RT−qPCR detection results of SIRT1 in the liver (Fig. 8B) and bioinformatics from TargetScan and miRanda, an interaction was speculated between miR-138-5p and SIRT1 mRNA. Accordingly, certain interaction sites existed between miR-138-5p and SIRT1 mRNA according to the TargetScan and miRDB databases (Fig. 9F). The interactions between miR-138-5p and SIRT1 were further confirmed by a dual-luciferase reporter gene assay.

In Fig. 9G, the relative fluorescence values of the mmu-miR-138-5p + SIRT1-WT co-transfection group were lower ($P < 0.05$) than those of the miR-NC + SIRT1-WT group. Upon mutation of SIRT1 mRNA, no difference in relative fluorescence was observed ($P > 0.05$). The above results validated that interaction sites existed between miR-138-5p and SIRT1 mRNAs.

3.8. *MiR-138-5p targeted SIRT1 and inhibited FXR acetylation*

Mechanistic studies showed that miR-138-5p directly targeted the 5′-UTR of SIRT1 mRNA (Fig. 9G). On the other hand, FXR activity was brought into play through the deacetylase action of SIRT1 [14]. Therefore, these results indicated that the downregulation of miR-138-5p modulated by kaempferol and nicotiflorin weakly suppressed SIRT1 mRNA expression, thereby enhancing the deacetylation of acetyl-FXR protein and activating FXR function (Fig. 8A–B). Therefore, all the above results further revealed that kaempferol and nicotiflorin significantly regulated liver damage induced by alcohol via the miR138-5p-SIRT1-FXR axis.

3.9. *Kaempferol and nicotiflorin significantly alleviated the gut microbiota structure at the phylum and genus levels*

Species-structure analysis is conducted by statistical methods to determine the dominant species present at every level of sample, as well as the relative abundance of every dominant species. This experiment focused on analyzing the phylum and genus levels. We explored the effects of kaempferol and nicotiflorin on the structure of the gut microbiota in chronic ALD mice at the phylum level.

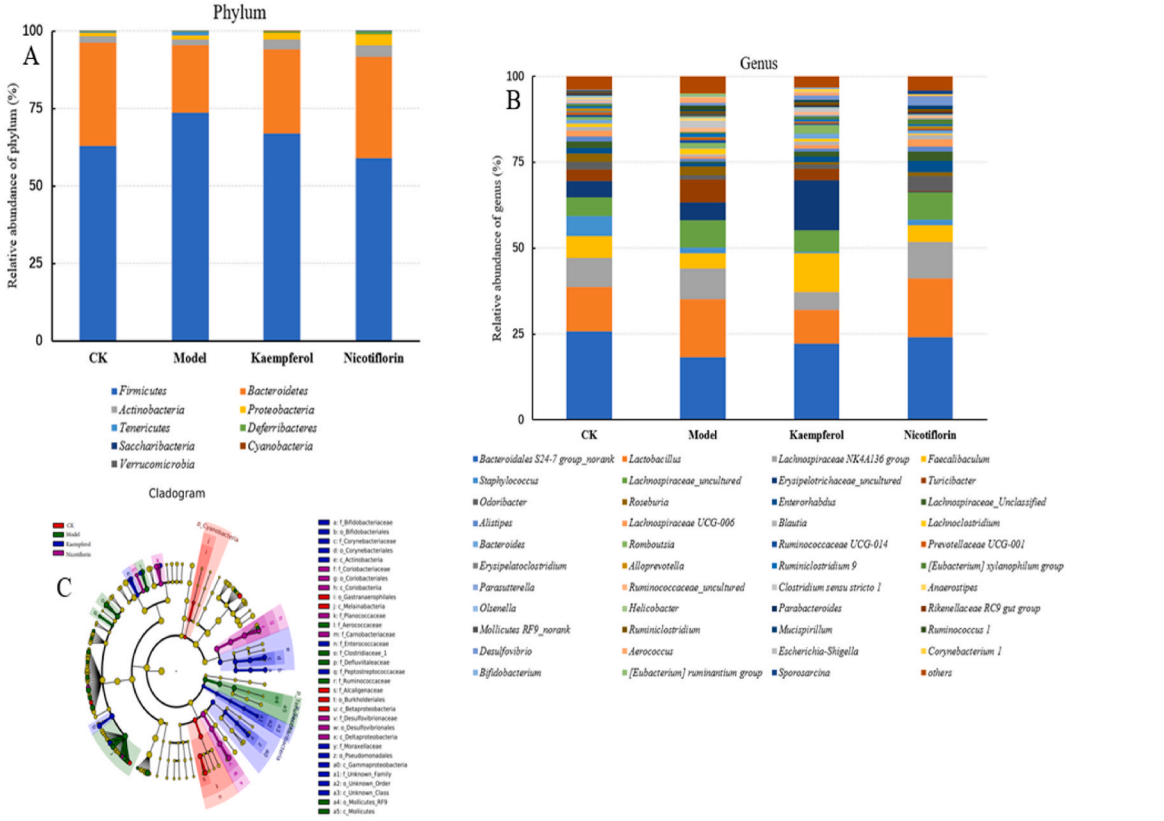

Fig. 10. (A) Histogram of phylum-level species composition analysis of gut bacteria in mice. (B) Histogram of analysis of genus-level species composition of the mouse gut bacteria. (C) Analysis of differences in gut bacteria at phylum level among the four groups.

Fig. 10A shows that the relative abundances of *Firmicutes*, *Bacteroidota*, *Verrucomicrobiota*, *Pseudomonadota*, *Actinomycetota*, *Deferribacteraceae*, etc., were higher in the mouse colon, among which the highest abundances of *Firmicutes* and *Bacteroidota* were observed. The two bacterial phyla exceeded 90 % in relative abundance. Compared with CK, the abundance of *Firmicutes* in the Model group increased by 16.55 %, whereas that of *Bacteroidota* decreased by 33.46 %. Compared with the model group, the abundance of *Firmicutes* in the kaempferol group decreased by 8.89 %, and the abundance of *Bacteroidota* increased by 22.96 %. The abundance of *Firmicutes* decreased by 19.78 % in the nicotiflorin group, and that of *Bacteroidota* increased by 48.50 %. Among them, the abundance of gut microbiota in mice effectively increased in the nicotiflorin group.

The genus level is shown in Fig. 10B and Fig. 10C, *Ruminococcaceae*_uncultured, *Ruminococcaceae* UCG-014, *Ruminococcus* 1 and *Ruminiclostridium* 9, *Parabacteroides*, *Bacteroidales* S24-7 group_norank, *Turicibacter*, *Roseburia*, *Clostridium sensu stricto* 1, Aerococcus, Enterorhabdus, *Mollicutes* RF9_norank, *Prevotellaceae* UCG-001, *Anaerostipes*, *Blautia*, *Faecalibaculum*, *Lachnospiraceae* UCG-006, *Lachnospiraceae*_Unclassified, *Lachnoclostridium*, and other bacterial genera exhibited relatively high abundances in the mouse cecal intestine. *Roseburia*, *Turicibacter*, and *Lachnospiraceae* under *Lachnoclastridium* were also the dominant genera with the highest abundance in the Model group, and the sum of the three genera accounted for approximately 11 % (Fig. 11A–C). *Bacteroides*, *Faecalibaculum*, *Enterorhabdus*, and *Lachnospiraceae*_ Unclassified were the dominant genera in the kaempferol and nicotiflorin groups. Among them, the sum of the abundances of the four genera in the kaempferol group was approximately 37 % (Fig. 11D–G). The sum of the abundances of the four genera in the nicotiflorin group was approximately 35 % (Fig. 11D–G).

4. Discussion

According to related research, long-term alcohol intake can cause ALD. Oxidative stress is an important cause of chronic alcoholic liver injury due to reactive oxygen species (ROS) overproduction [15]. It is proved that excess ROS increase MDA production, activate lipid peroxidation and indicate the degree of cell damage [16]. In addition, relevant research proves that alcohol-induced oxidative stress can be protected by balancing ROS and antioxidant enzymes. Antioxidant enzymes such as SOD and GSH can improve lipid peroxidation, reduce the level of reactive oxygen species and free radicals in cells, and maintain the structure and function of cell membranes [17]. The results of our study showed that kaempferol and nicotiflorin could significantly increase of the SOD and GSH levels. Furthermore, highly active FXR has been shown to decrease CYP2E1 and SREBP-1c levels and reduce oxidative stress and lipid metabolism in alcohol-fed mice [18]. The pathogenesis of alcoholic liver injury is related to microsomal ethanol oxidation system

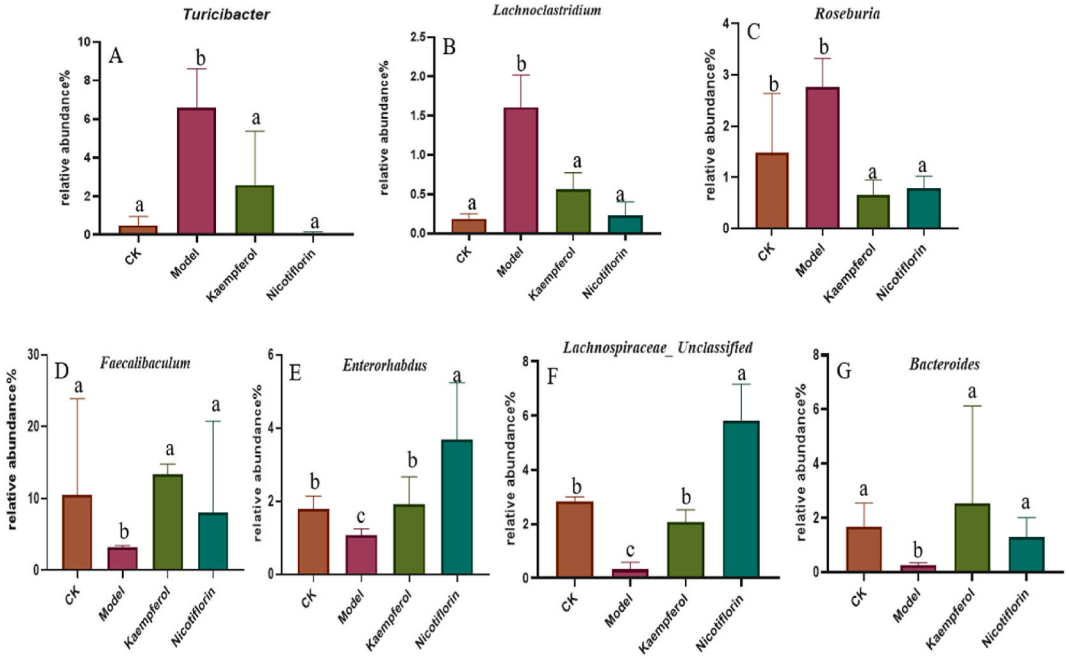

Fig. 11. (A–C) qPCR analysis of *Roseburia*, *Turicibacter*, and *Lachnospiraceae* under Lachnoclastridium in feces. (D–G) qPCR analysis of *Bacteroides*, *Faecalibaculum*, *Enterorhabdus*, and *Lachnospiraceae_* Unclassified in feces.
Note: ($n = 5$) The same letters indicate no significant difference between groups ($p > 0.05$), and different letters indicate significant differences between groups ($p < 0.05$).

(MEOS). CYP2E1 is an important part of MEOS, which is a hemoglobin containing heme involved in the reaction [19]. CYP2E1 metabolizes ethanol to produce acetaldehyde or ROS. This is related to ethanol-induced ALD. The induction of CYP2E1 promotes oxidative stress and leads to lipid peroxidation, contributing to the development of liver damage [20–23]. Knocking out CYP2E1 or administering a CYP2E1 inhibitor significantly reduced the severity of ALD [23]. The results of our study showed that Kaempferol and nicotiflorin could significantly suppress the abnormal increase of CYP2E1 level caused by alcoholic liver injury.

In recent studies, ALD was shown to lead to the abnormal expression of miRNAs in the liver [24]. Fluorescein reporter gene assay results showed that miR-138-5p regulates SIRT1. miR-138-5p inhibits oxidative stress and regulates the inflammatory response and lipid metabolism by regulating the expression of deacetylase SIRT1 [25,26]. Kaempferol and nicotiflorin also regulated FXR activity through the miR-138-5p-SIRT1 axis to exert a protective effect on ALD. The high expression of miR-138-5p and the low expression of deacetylase SIRT1 induced by ethanol resulted in decreased FXR activity, which in turn affected downstream oxidative stress and lipid metabolism. Therefore, the protection of ALD by kaempferol and nicotiflorin was strongly associated with miR-138-5p/SIRT1 axis modulation. This study suggested that the potential pathogenesis of alcoholic liver injury could be further studied by exploring the miRNA related to alcoholic liver disease in the liver.

It is proved that the gut microbiota was shown to be extremely important in the pathogenesis of alcoholic liver injury [27]. Intestinal bacteria or their metabolites enter the liver through the portal vein [28], resulting in changes in the intestinal microflora and affecting liver function [29,30]. *Roseburia* has been reported as a potential causative factor [31]. The abundance of *Lachnoclostridium* in the gut microbiota of patients with liver injury also obviously increases, and the abundance of *Turicibacter* in the gut microbiota of patients with intestinal disease significantly increases [32–34]. Our current findings showed that the abundance of the *Roseburia*, *Lachnoclostridium*, and *Turicibacter* genera of the gut microbiota in model group mice significantly increased, indicating that it may be a class of bacteria that aggravates chronic ALD. Therefore, our study proved that there was a certain relationship between intestinal flora and the pathogenesis of alcoholic liver disease. The focus of future research should explore the intestinal flora related to alcoholic liver injury, and prevent or treat alcoholic liver injury by intervening the related flora in a certain way.

5. Conclusions

The dominant flavonoids kaempferol and nicotiflorin reduced alcohol-induced liver damage by enhancing alcohol metabolism and reducing oxidative stress and lipid metabolism, which were all associated with FXR deacetylation. The modulation of FXR activity was again strongly associated with the miR-138-5p/SIRT1 axis. In addition, the alleviation of intestinal microorganism disorder by kaempferol and nicotiflorin also ameliorated alcohol-induced liver injury. Therefore, *T. hemsleyanum* may have broad application prospects in protection against alcoholic liver injury. However, there is no detailed comparison of the differences between the two components in protecting liver injury. At the same time, there is no further comparative analysis of the structure-activity relationship

of different *Tetrastigma hemsleyanum* flavonoids in protecting alcoholic liver injury. And the further research should be investigated in future.

Ethics statement

The animal experiments protocol was approved according to the agreement of Laboratory Animal Ethics Committee from China Jiliang University (2023-003), and all animal procedures were performed in accordance with the institutional and national guidelines.

Funding

This work was supported financially by the National Natural Science Foundation of China (31100499), the Major Science and Technology Projects in Zhejiang Province (2020C02045) and Zhejiang Science and Technology Commissioner Team Project.

Data availability

Data will be made available on request.

CRediT authorship contribution statement

Jian Ge: Writing – review & editing, Supervision, Conceptualization. **Guangmei Li:** Writing – original draft, Methodology, Data curation. **Zhaowen Chen:** Writing – original draft, Methodology, Data curation. **Weijia Xu:** Formal analysis, Data curation. **Xuanhao Lei:** Software, Formal analysis, Data curation. **Shengnan Zhu:** Software, Formal analysis, Data curation.

Declaration of competing interest

The authors declare that they have no known competing financial interests or personal relationships that could have appeared to influence the work reported in this paper.

Acknowledgments

We are grateful to Zonghua Dong, Luting Ye, Simin Ren, Min Cheng and Xuanxuan Zou (College of Life Sciences, China Jiliang University) for generously providing rat administration. Financial assistance from the National Natural Science Foundation of China and the Major Science and Technology Projects in Zhejiang Province are sincerely appreciated.

Abbreviations

ALDs	Alcoholic liver diseases
ALT	Alanine *trans*-aminase
AST	Aspartate transaminase
BCA	Bicinchoninic acid assay
BW	Beijing Red Star wine
CK	Control
CMC-Na	Carboxymethylcellulose sodium
CYP2E1	Cytochrome P450 2E1
ELISA	Enzyme-linked immunosorbent assay
EVs	Extracellular vehicles
FXR	Farnesoid X receptor
GADPH	Glyceraldehyde-3-phosphate dehydrogenase
GSH	Reduced glutathione
GSH-Px	Glutathione peroxidase
H&E	Hematoxylin–eosin
HPLC	High-performance liquid chromatography
ICR	Institute of Cancer Research
K	Kaempferol
M	Model
MEOS	Microsomal ethanol oxidation system
MDA	Malondialdehyde
Mut	Mutant
N	Nicotiflorin
PBS	Phosphate buffer saline
PCR	Polymerase chain reaction

PVDF Polyvinylidene difluoride
ROS Reactive oxygen species
RT-qPCR Quantitative real-time PCR assay
SIRT1 Silencing information regulator 2 related enzyme-1
SOD Superoxide dismutase
SREBP-1c Sterol regulatory element binding protein 1c
TC Total cholesterol
TG Triglyceride
WB Western blot assay
WT Wild-type

Appendix A. Supplementary data

Supplementary data to this article can be found online at https://doi.org/10.1016/j.heliyon.2023.e23336.

References

[1] B. Gao, R. Bataller, Alcoholic liver disease: pathogenesis and new therapeutic targets, Gastroenterology 141 (5) (2011) 1572–1585, https://doi.org/10.1053/j.gastro.2011.09.002.
[2] J. Altamirano, R. Bataller, Alcoholic liver disease: pathogenesis and new targets for therapy, Nat. Rev. Gastroenterol. Hepatol. 8 (1) (2011) 491–501, https://doi.org/10.1038/nrgastro.2011.134.
[3] M.A. Avila, J.F. Dufour, A.L. Gerbes, et al., Recent advances in alcohol-related liver disease (ALD): summary of a Gut round table meeting, Gut 69 (4) (2020) 764–780, https://doi.org/10.1136/gutjnl-2019-319720.
[4] J.S. Bajaj, Alcohol, liver disease and the gut microbiota, Nat. Rev. Gastroenterol. Hepatol. 16 (1) (2019) 235–246, https://doi.org/10.1038/s41575-018-0099-1.
[5] L. Qian, D. Dai, H. Jiang, W. Lin, Research progresses of the endangered medicinal plant *Tetrastigma hemsleyanum* Diels et Gilg, Acta Agric. Zhejiangensis 27 (2015) 1301–1308.
[6] B. Zhu, C. Qian, F. Zhou, J. Guo, et al., Antipyretic and antitumor effects of a purified polysaccharide from aerial parts of *Tetrastigma hemsleyanum*, J. Ethnopharmacol. 253 (2020), 112663, https://doi.org/10.1016/j.jep.2020.112663.
[7] W. Hu, Y. Zheng, P. Xia, Z. Liang, The research progresses and future prospects of *Tetrastigma hemsleyanum* Diels et Gilg: a valuable Chinese herbal medicine, J. Ethnopharmacol. 271 (2021), 113836, https://doi.org/10.1016/j.jep.2021.113836.
[8] G. Li, J. Ge, Y. Zheng, et al., *Tetrastigma hemsleyanum* Diels et Gilg roots from different origins: pharmacognostical identification, content determination of functional composition and in vitro antioxidant activity, J. Am. J. Biochem. Biotech. 19 (1) (2023) 36–46, https://doi.org/10.3844/ajbbsp.2023.36.46.
[9] X. Huang, S. Zhang, Y. Li, et al., Insight into the binding characteristics of rutin and alcohol dehydrogenase: based on the biochemical method, spectroscopic experimental and molecular model, J. Photochem. Photobiol. B Biol. 228 (2022), 112394, https://doi.org/10.1016/j.jphotobiol.2022.112394.
[10] H. Lin, X. Guo, J. Liu, et al., Improving lipophagy by restoring Rab7 cycle: protective effects of quercetin on ethanol-induced liver steatosis, J. Nutrients 14 (3) (2022), https://doi.org/10.3390/nu14030658, 658-658.
[11] S. Lee, J. Lee, H. Lee, et al., Relative protective activities of quercetin, quercetin-3-glucoside, and rutin in alcohol-induced liver injury, J. Food Biochem. 43 (11) (2019), 13002, https://doi.org/10.1111/jfbc.13002.
[12] S. Liu, L. Tian, G. Chai, et al., Targeting heme oxygenase-1 by quercetin ameliorates alcohol-induced acute liver injury via inhibiting NLRP3 inflammasome activation, J. Food & function. 9 (8) (2018) 4184–4193, https://doi.org/10.1039/C8FO00650D.
[13] M. Wang, J. Sun, Z. Jiang, et al., Hepatoprotective effect of kaempferol against alcoholic liver injury in mice, Am. J. Chinese Med. 43 (2) (2015) 241–254, https://doi.org/10.1142/S0192415X15500160.
[14] J.K. Kemper, Z. Xiao, B. Ponugoti, et al., FXR acetylation is normally dynamically regulated by p300 and SIRT1 but constitutively elevated in metabolic disease states, J. Cell Metabolism 10 (5) (2009) 392–404, https://doi.org/10.1016/j.cmet.2009.09.009.
[15] S.D. Minicis, D.A. Brenner, Oxidative stress in alcoholic liver disease: role of NADPH oxidase complex, J. Gastroenterol. Hepatol. 23 (1) (2008) 98–103, https://doi.org/10.1111/j.1440-1746.2007.05277.x.
[16] C.J. Weydert, J.J. Cullen, Measurement of superoxide dismutase, catalase and glutathione peroxidase in cultured cells and tissue, Nat. Protoc. 5 (1) (2010) 51–66, https://doi.org/10.1038/nprot.2009.197.
[17] P. Chen, P. Stärkel, J.R. Turner, S.B. Ho, B. Schnabl, Dysbiosis-induced intestinal inflammation activates tumor necrosis factor receptor I and mediates alcoholic liver disease in mice, Hepatology (Baltimore, Md 61 (3) (2015) 883–894.
[18] W. Wu, B. Zhu, X. Peng, et al., Activation of farnesoid X receptor attenuates hepatic injury in a murine model of alcoholic liver disease, J. Biochemi. Biophys. Res. Commun. 443 (1) (2014) 68–73, https://doi.org/10.1016/j.bbrc.2013.11.057.
[19] R. Harjumäki, C.S. Pridgeon, M. Ingelman-Sundberg, CYP2E1 in alcoholic and non-alcoholic liver injury. Roles of ROS, reactive intermediates and lipid overload, Int. J. Mol. Sci. 22 (15) (2021) 8221, https://doi.org/10.3390/ijms22158221.
[20] Y. Shi, Y. Liu, S. Wang, et al., Endoplasmic reticulum-targeted inhibition of CYP2E1 with vitamin E nanoemulsions alleviates hepatocyte oxidative stress and reverses alcoholic liver disease, Biomaterials 288 (2022), 121720, https://doi.org/10.1016/j.biomaterials.2022.121720.
[21] S. Sutti, C. Rigamonti, M. Vidali, et al., CYP2E1 autoantibodies in liver diseases, Redox Biol. 3 (2014) 72–78, https://doi.org/10.1016/j.redox.2014.11.004.
[22] A. Butura, K. Nilsson, K. Morgan, T.R. Morgan, S.W. French, I. Johansson, I. Schuppe-Koistinen, M. Ingelman-Sundberg, The impact of CYP2E1 on the development of alcoholic liver disease as studied in a transgenic mouse model, J. Hepatol. 50 (3) (2009) 572–583, https://doi.org/10.1016/j.jhep.2008.10.020.
[23] Y. Lu, J. Zhuge, X. Wang, J. Bai, A.I. Cederbaum, Cytochrome P450 2E1contributes to ethanol-induced fatty liver in mice, Hepatology 47 (5) (2008) 1483–1494, https://doi.org/10.1002/hep.22222.
[24] T. Xu, L. Li, H. Hu, et al., MicroRNAs in alcoholic liver disease: recent advances and future applications, J. Cellular Physiol. 234 (1) (2018) 382–394, https://doi.org/10.1002/jcp.26938.
[25] Y. Liu, M. Zhang, H. Zhang, et al., Anthocyanins inhibit airway inflammation by downregulating the NF-κB pathway via the miR-138-5p/SIRT1 Axis in asthmatic mice, J. Int. Archives Allergy Immunol. 183 (5) (2022) 539–551, https://doi.org/10.1159/000520645.
[26] S. Guo, B. Ma, X. Jiang, et al., Astragalus polysaccharides inhibits tumorigenesis and lipid metabolism through miR-138-5p/SIRT1/SREBP1 pathway in prostate cancer, J. Front. Pharmacol. 11 (2020), https://doi.org/10.3389/fphar.2020.00598.
[27] G. Vassallo, A. Mirijello, A. Ferrulli, et al., Review article: alcohol and gut microbiota - the possible role of gut microbiota modulation in the treatment of alcoholic liver disease, J. Alimentary Pharmacol. Therapeutic. 41 (10) (2015) 917–927, https://doi.org/10.1111/apt.13164.
[28] S. Leclercq, S. Matamoros, P.D. Cani, et al., Intestinal permeability, gut-bacterial dysbiosis, and behavioral markers of alcohol-dependence severity, J. Proc. Nation. Acad. Sci. USA 111 (42) (2014) E4485–E4493, https://doi.org/10.1073/pnas.1415174111.

[29] V.B. Dubinkina, A.V. Tyakht, V.Y. Odintsova, et al., Links of gut microbiota composition with alcohol dependence syndrome and alcoholic liver disease, J. Microbiome. 5 (1) (2017) 141, https://doi.org/10.1186/s40168-017-0359-2.
[30] C. Martino, L.S. Zaramela, B. Gao, et al., Acetate reprograms gut microbiota during alcohol consumption, J. Nat. Commun. 13 (1) (2022) 4630, https://doi.org/10.1038/s41467-022-31973-2.
[31] B. Seo, K. Jeon, S. Moon, et al., Roseburia spp. abundance associates with alcohol consumption in humans and its administration ameliorates alcoholic fatty liver in mice, J. Cell Host & Microbe 27 (1) (2020) 25–40, https://doi.org/10.1016/j.chom.2019.11.001.
[32] G. Wang, Y. Zhang, R. Zhang, et al., The protective effects of walnut green husk polysaccharide on liver injury, vascular endothelial dysfunction and disorder of gut microbiota in high fructose-induced mice, J. Int. J. Biolog. Macromol. 162 (2020) 92–106, https://doi.org/10.1016/j.ijbiomac.2020.06.055.
[33] C. Li, L. Cui, X. Wang, et al., Using Gut microbiota to distinguish non-alcoholic steatohepatitis from non-alcoholic fatty liver, J. Int. Med. Res. 48 (12) (2020), https://doi.org/10.1177/0300060520978122.
[34] L. Shang, H. Liu, H. Yu, et al., Core altered microorganisms in colitis mouse model: a comprehensive time-point and fecal microbiota transplantation analysis, J. Antibiotics (Basel, Switzerland) 10 (6) (2021) 643, https://doi.org/10.3390/antibiotics10060643.